An MRAS Speed Observer Based on Control Winding Flux for Sensorless Control of Stand-Alone BDFIGs

Wei Xu, *Senior Member, IEEE*, Alameen K. Ebraheem, Yi Liu, *Member, IEEE*, Jianguo Zhu, *Senior Member, IEEE*, Mohamed G. Hussien, and Omer Mohammed Elbabo Mohammed

***Abstract*—This article presents a new rotor speed observer for the sensorless control of stand-alone brushless doubly fed induction generators based on the control winding flux model reference adaptive system structure. The observer is incorporated in the control strategy for regulating the terminal voltage magnitude and frequency under the different operating conditions. The capability of the proposed observer and control method is demonstrated by comprehensive simulation results and verified by experiments. As shown, without using physical speed sensors, the sensorless control algorithm incorporating the proposed speed observer can effectively maintain the amplitude and frequency of power winding voltage constant at different rotor speeds and under different conditions of load and machine parameter, e.g., inductance and/or resistance, variations.**

***Index Terms*—Brushless doubly fed induction generators (BDFIGs), model reference adaptive system (MRAS), sensorless control, speed observer.**

NOMENCLATURE

ω_1, ω_2	Angular frequencies of power and control windings (electrical rad/s).
$\tilde{\omega}_r, \omega_r$	Estimated and actual rotor angular speeds (mechanical rad/s).
p_1, p_2	Pole pairs of power and control windings.
u, i, ψ	Voltage (V), current (A), and flux linkage (Wb).
U	RMS value of voltage (V).
R_r, R_1, R_2	Resistances of the rotor, power and control windings (Ω).
L_r, L_1, L_2	Self-inductances of the rotor, power and control windings (H).
L_{1r}, L_{2r}	Mutual inductances between the rotor and power windings, and the rotor and control windings (H).
$\tilde{\theta}_r, \theta_r$	Measured and estimated rotor positions (mechanical rad).
S	Differential operator.

Manuscript received July 1, 2019; revised October 3, 2019; accepted November 11, 2019. Date of publication November 19, 2019; date of current version March 13, 2020. This work was supported in part by the National Natural Science Foundation of China under Grants 51707079, 51877093, and 51807075, and in part by the National Key Research and Development Program of China under Grant 2018YFE0100200. Recommended for publication by Associate Editor D. G. Xu. *(Corresponding author: Yi Liu.)*

W. Xu and Y. Liu are with the State Key Laboratory of Advanced Electromagnetic Engineering and Technology, School of Electrical and Electronic Engineering, Huazhong University of Science and Technology, Wuhan 430074, China (e-mail: weixu@hust.edu.cn; liuyi82@hust.edu.cn).

A. K. Ebraheem is with the State Key Laboratory of Advanced Electromagnetic Engineering and Technology, School of Electrical and Electronic Engineering, Huazhong University of Science and Technology, Wuhan 430074, China, and also, with the Faculty of Engineering and Technology, Nile Valley University, River Nile, Atbara, Sudan (e-mail: elaminkamal33@yahoo.com).

J. Zhu is with the School of Electrical and Information Engineering, University of Sydney, Sydney, NSW 2006, Australia (e-mail: jianguo.zhu@sydney.edu.au).

M. G. Hussien and O. M. Elbabo Mohammed are with the State Key Laboratory of Advanced Electromagnetic Engineering and Technology, School of Electrical and Electronic Engineering, Huazhong University of Science and Technology, Wuhan 430074, China (e-mail: mohamed.hussien3@f-eng.tanta.edu.eg; babo271@yahoo.com).

Color versions of one or more of the figures in this article are available online at http://ieeexplore.ieee.org.

Digital Object Identifier 10.1109/TPEL.2019.2954990

I. INTRODUCTION

BECAUSE of the use of slip ring and brushes, the traditional doubly fed induction generator (DFIG) suffers from various drawbacks, such as large size, low reliability, and high cost required for the maintenance. On the other hand, the brushless doubly fed induction generator (BDFIG) has attracted a lot of attention due to its low maintenance cost and high reliability structure. The power winding (PW) and the control winding (CW) with different numbers of pole pairs to prevent the direct coupling between them are housed in the same stator of the BDFIG, and the rotor is specially designed to offer the cross coupling between the PW and CW [1]–[3]. BDFIG can avoid all drawbacks of DFIG as it does not require any brushes [4]. The stand-alone BDFIG as a power generator has been widely used in variable-speed constant-frequency generation systems, e.g., ship shaft power generation applications [4]. The BDFIG as a stand-alone system should be controlled to keep the PW voltage constant to support the loads. In order to eliminate the use of a delicate physical speed sensor, to improve the reliability, a speed estimator can be used [5]. The delicate encoders are especially prone to damage due to the vibrations caused by the main energy source such as a combustion engine or a wind turbine [6]. Therefore, the sensorless control without using any physical velocity and position sensors is a very strong merit. Due to its excellent performance, computational simplicity, and straightforward stability approach, the model reference adaptive system (MRAS) is a more and more popular strategy of the sensorless control schemes [7].

The direct voltage control (DVC) of BDFIG has been presented in many works of literature [1], [2], [8]–[11] based on the sensored control algorithm. In addition, in [12]–[14], the sensorless control of DFIG is presented, and that of BDFIG is represented in [15]–[20]. While the principles of MRAS observers for DFIGs have been well presented in the literature, only a few literatures have dealt with MRAS for BDFIGs [15], [20]. In [1], the quality of output voltage is improved for the stand-alone BDFIG system using the active front-end rectifier. In [2], the active and reactive powers are controlled for BDFIG connected to an unbalanced grid using a vector control (VC) strategy. In [3] and [4], with load and rotor speed variation, the frequency and amplitude of the PW voltage are kept constant by controlling the CW current amplitude and frequency for the ship shaft power generation. In [10], an improved DVC for BDFIG as a stand-alone system under the balanced loads has been presented. In [11], a VC strategy has been proposed for the DVC of ship shaft BDFIG system under two schemes, the PW voltage-oriented control and the field orientation of PW with a complete comparison between them. The sensorless VC of DFIG for both stand-alone and grid-connected operations has been presented in [12], which is based on the MRAS observer using the current and flux of both stator and rotor. Also, a new sensorless control method of DFIG based on the MRAS observer using a rotor current has been presented in [13]. Based on the MRAS observer using the reactive power, the slip frequency is observed in [14] for the stand-alone DFIG system and is used for back EMF compensation in the rotor current controller. In [15], the stator PW flux-oriented VC for the grid-connected BDFIG is presented using an MRAS observer. On the other hand, in [16], the PW voltage is controlled by using a sensorless DVC method. In contrary to [16], the feed-forward compensation method is presented for the unbalanced loads in [17]. Based on the rotor speed observer presented in [18], a sensorless control strategy by feeding the unbalanced and nonlinear loads for the BDFIG in a ship shaft generation system has been presented in [19].

Two previous studies on this subject have been presented in [20] and [21]. The first difference of the three methods, [20], [21] and the proposed MRAS in this article, lies in the control target. The control targets of the methods in [20] and this article are the same including the DVC of the stand-alone BDFIG systems in terms of the voltage amplitude and frequency without any speed sensors, whereas the control target of the method in [21] is the speed control of brushless doubly-fed induction machine (BDFIM) without using any speed sensors.

The second difference among the three methods is the principle of implementation. The method in [20] employs the PW flux as the control component with integrators to calculate the intended flux in its stationary frame. In [21], the CW current is estimated in the stationary frame and used as the control component. In the proposed method, in this article, the CW flux is considered as the control component, without the need of the integrator to obtain the intended flux, based on the rotatory frame. Finally, the number of integrators in the speed observer used in [20], [21], and the proposed method in this article is four, four, and two, respectively.

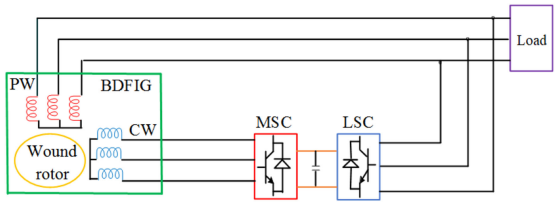

Fig. 1. Structure of BDFIG.

Based on the analysis above, the method proposed in this manuscript can be regarded as the most preferred one among the three methods due to the use of the fewest number of integrators and the consequent lowest complexity in the calculation's operation.

In this article, the CW-flux MRAS-based voltage-oriented control scheme is used to achieve the sensorless control of the stand-alone BDFIG systems. The proposed method contains two models, the adaptive model and the reference model using the CW flux.

This article is organized as follows. The mathematical model of BDFIG is described in Section II. The complete design of the proposed MRAS observer is presented in Section III. Section IV presents the proposed sensorless control system based on the CW-flux MRAS observer. The proposed strategy is simulated in Section V and verified by experiments in Section VI. Finally, Section VII concludes this article.

II. Mathematical Model

In the BDFIG system, the stator PW is directly connected to the load terminals, and the CW is connected to the load side via a back-to-back converter, as illustrated in Fig. 1.

In the synchronous mode, the rotor speed of BDFIG can be expressed as [19]

$$\omega_r = \frac{\omega_1 + \omega_2}{p_1 + p_2}. \tag{1}$$

The mathematical vector model of BDFIG in the dq synchronous frame can be derived as [19]

$$u_1 = R_1 i_1 + \frac{d\psi_1}{dt} + j\omega_1 \psi_1 \tag{2}$$

$$0 = R_r i_r + \frac{d\psi_r}{dt} + j(\omega_1 - p_1\omega_r)\psi_r \tag{3}$$

$$u_2 = R_2 i_2 + \frac{d\psi_2}{dt} + j(\omega_1 - (p_1 + p_2)\omega_r)\psi_2 \tag{4}$$

$$\psi_1 = L_1 i_1 + L_{1r} i_r \tag{5}$$

$$\psi_r = L_r i_r + L_{2r} i_2 + L_{1r} i_1 \tag{6}$$

$$\psi_2 = L_2 i_2 + L_{2r} i_r. \tag{7}$$

III. MRAS Observer Design

The proposed MRAS observer, as shown in Fig. 2, has two models, the adaptive model and the reference model. The measured stator CW flux obtained from the voltages and currents of the PW is compared with the flux obtained from the PW and CW stator currents. The error is controlled to be equal to zero

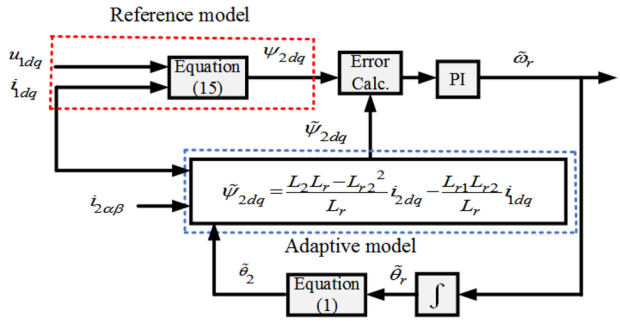

Fig. 2. Block diagram of the CW-flux MRAS observer.

using a PI controller and the output of this controller is used as the estimation of the rotor speed. Then, this estimated speed is fed back to adjust the adaptive model.

The adaptive model can be derived by the procedure as follows. Substituting (6) into (3), the rotor current i_r can be obtained by

$$i_r = \frac{-[s + j(\omega_1 - p_1\omega_r)](L_{2r}i_2 + L_{1r}i_1)}{R_r + [s + j(\omega_1 - p_1\omega_r)]L_r} = \frac{\frac{L_{2r}}{L_2}\psi_2 + L_{1r}i_1}{-\frac{R_r}{s+j(\omega_1 - p_1\omega_r)} - L_r + \frac{L_{2r}^2}{L_2}}. \quad (8)$$

In order to employ a fractionally rated power converter to drive the stand-alone BDFIG system, the CW angular frequency ω_2 is usually limited to 30% of the PW frequency. According to (1), the range of the ω_r would be between 70% and 130% of ω_1. In terms of the BDFIG with the typical pole pairs of 1 and 3 for PW and CW, the value of $\omega_1 - p_1\omega_r$ would be in the range of (67.5%–82.5%)ω_1. In general, the value of ω_1 is 100π or 120π rad/s. Hence, the value of $(\omega_1 - p_1\omega_r)$ will be much greater than R_r, and then it can be concluded that the term $R_r/[s + j(\omega_1 - p_1\omega_r)]$ can be approximately ignored at steady state. Then, from (8), the rotor current can be expressed as

$$i_r = \frac{L_{2r}\psi_2 + L_2L_{1r}i_1}{{L_{2r}}^2 - L_2L_r}. \quad (9)$$

Substituting (9) into (7), the CW stator flux can be obtained as

$$\psi_2 = \frac{L_2L_r - L_{2r}^2}{L_r}i_2 - \frac{L_{1r}L_{2r}}{L_r}i_1. \quad (10)$$

Consequently, the adaptive model to estimate the CW stator flux can be obtained as

$$\tilde{\psi}_{2dq} = \frac{L_2L_r - L_{2r}^2}{L_r}i_{2dq} - \frac{L_{1r}L_{2r}}{L_r}i_{1dq}. \quad (11)$$

In the steady state, $d\psi_r/dt = 0$. And then, from (3), the rotor flux at steady state can be derived as

$$\psi_r = -\frac{R_r i_r}{j(\omega_1 - p_1\omega_r)}. \quad (12)$$

When i_r is below or equal to the rated value in the steady state, $(\omega_1 - p_1\omega_r) \gg R_r i_r$, and the rotor flux can also be ignored.

From (6), by ignoring the effect of rotor flux, the rotor current can be obtained by

$$i_r = -\frac{L_{2r}}{L_r}i_2 - \frac{L_{1r}}{L_r}i_1. \quad (13)$$

From (13) and (5), the CW current can be written as

$$i_2 = -\frac{L_r}{L_{2r}L_{1r}}\psi_1 + \frac{L_rL_1 - L_{1r}^2}{L_{1r}L_{2r}}i_1. \quad (14)$$

Substituting (9) and (14) into (7), the reference model of the CW stator flux can be obtained as

$$\psi_{2dq} = \frac{L_{2r}^2 - L_2L_r}{L_{1r}L_{2r}}\psi_{1dq} + \frac{L_2L_1L_r - L_1L_{2r}^2 - L_2L_{1r}^2}{L_{1r}L_{2r}}i_{1dq}. \quad (15)$$

From (2), the PW stator flux in the dq reference frame at the steady state can be expressed as

$$\begin{cases} \psi_{1d} = \frac{u_{1q} - R_1 i_{1q}}{\omega_1} \\ \psi_{1q} = -\frac{u_{1d} - R_1 i_{1d}}{\omega_1}. \end{cases} \quad (16)$$

The rotor speed can be estimated as

$$\tilde{\omega}_r = (K_p + \frac{K_i}{S})(\tilde{\psi}_{2d}.\psi_{2q} - \psi_{2d}.\tilde{\psi}_{2q}) \quad (17)$$

where K_p and K_i are the proportional gain and the integral gain, respectively.

IV. Proposed Sensorless Control Based on the CW-Flux MRAS Observer

The main aim of the stand-alone systems is to control the output voltage in terms of the magnitude and frequency. Based on the proposed CW-flux MRAS observer, a sensorless control method for the stand-alone BDFIG system is proposed, which consists of five main parts, as shown in Fig. 3.

In the part of the PW voltage amplitude control, the amplitude of the voltage is controlled by a PI controller with the error between the reference and actual values of the PW voltage amplitude. The actual value of the PW voltage amplitude can be obtained from the part of the actual PW voltage amplitude calculating. The output of the PW voltage amplitude control is the d-axis component of the CW current. Another part is considered to obtain the voltage orientation in which the PW voltage q-axis component u_{1q} can converge to zero so that the resultant PW voltage vector can overlap the d-axis of the rotating dq frame. Consequently, the PW voltage and frequency can well track their reference values. For the d- and q-axis components of the PW voltage, PW and CW currents can be input to the CW-flux MRAS observer for obtaining the estimated rotor speed of the BDFIG. Then, in order to implement the coordinate transformation in the CW current control loop, the CW reference angle θ_2^* is obtained by integration of the estimated speed and the reference PW frequency according to (1). In the current control loop, in order to simplify the control scheme, the reference CW q-axis current i_{2q}^* is set to zero, which means that the CW d-axis current $i_{2\,d}{}^*$ would be equal to the amplitude reference value I_2^*.

The reference values of the three-phase CW voltages can be the output from the CW current control loop and sent to the space vector pulse width modulation (SVPWM) generator to generate

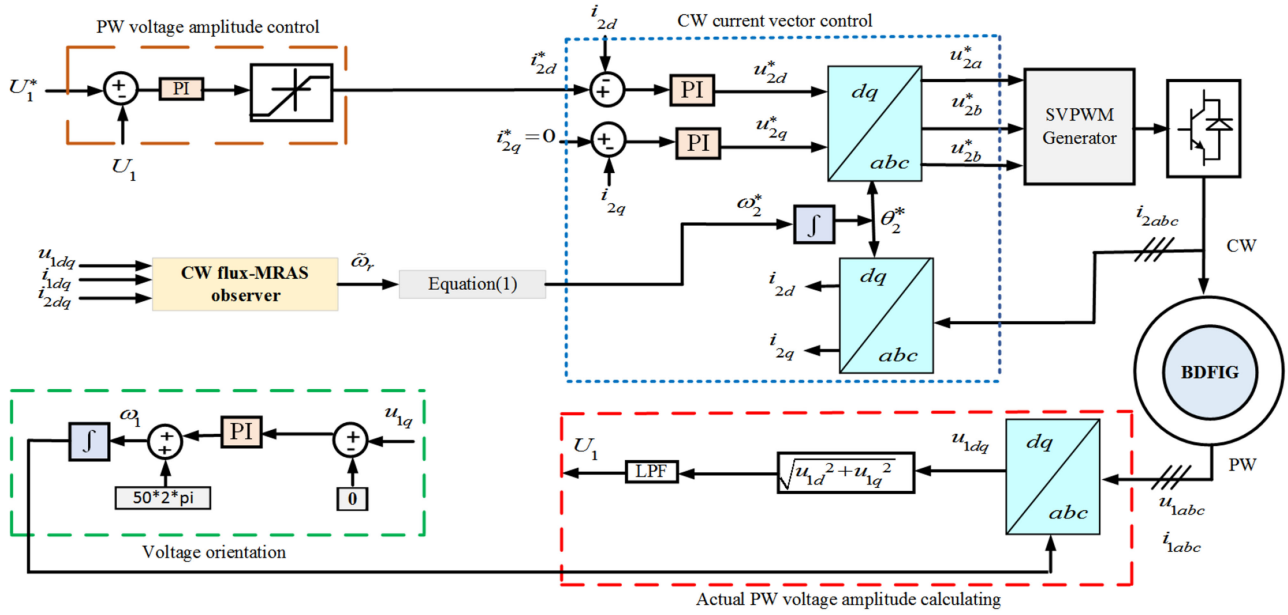

Fig. 3. Main block diagram of the proposed sensorless control method for the stand-alone BDFIG system.

TABLE I
DETAILED PARAMETERS OF BDFIG

Parameter	Value
Capacity	30 kVA
Range of speed	600 ~1200 rpm
p_1, p_2	1, 3
PW voltage and current	380 V, 45 A
CW voltage range	0~350 V
CW current range	0~40 A
R_1, R_2, R_r	0.4034 Ω, 0.2680 Ω, 0.3339 Ω
L_1, L_2, L_r	0.4749 H, 0.03216 H, 0.2252 H
L_{1r}, L_{2r}	0.3069 H, 0.02584 H

the correct CW voltage. Finally, the frequency and amplitude of the PW voltage are kept constant at the desired voltage and frequency (in this article, the reference values are set as 311 V and 50 Hz) under the variable rotor speed, load, and parameters for the stand-alone BDFIG system.

V. SIMULATION RESULTS

To demonstrate the capability of the proposed control method, some of the obtained simulation results are presented in this section for a BDFIG when the rotor speed varies from 700 to 600 r/min. The capability of the proposed CW-flux MRAS observer for the sensorless DVC when the parameters vary is also confirmed in this section. The parameters of the simulated system are listed in Table I.

A. Response Under Speed and Load Change

Fig. 4 illustrates the response when the rotor speed reduces from 700 to 600 r/min at 1 s for the proposed CW-flux MRAS observer under the constant three-phase resistive load. Fig. 5 shows the effect of load change, in which the applied load is started with a three-phase resistive load whose resistance equals 50 Ω per phase, then at 1 s, the load is changed suddenly to 25 Ω per phase. Fig. 4(a)–(e) illustrates the actual and estimated rotor speeds, the PW three-phase voltages during different periods, and the CW three-phase currents, respectively. Fig. 5(a)–(g) illustrates the actual and estimated rotor speeds, the speed percentage error, the PW three-phase voltages during different periods, the CW three-phase currents during different periods, and the PW active power, respectively.

The simulation results demonstrate good tracking performance for the frequency and voltage amplitude control when the rotor speed varies and the load changes. The presented simulation results verify that the estimated rotor speed is in good accordance with the measured speed.

This ensures the capability of the proposed CW-flux MRAS observer for the sensorless DVC control system of the stand-alone BDFIG.

B. Effect of Parameters Variations

Figs. 6 and 7 show the response of BDFIG, under the same load change condition, as presented in Fig. 5, when the PW resistance and inductances vary, respectively. This is studied with 130% of the PW resistance and 150% of the whole inductance values. As for the PW resistance mismatch, Fig. 6(a)–(g) illustrates the actual and estimated rotor speeds, the speed percentage error, the PW three-phase voltages and currents during different periods, and the PW active power, respectively. Fig. 7(a)–(g) illustrates these waveforms during the whole inductance variation. It can be dedicated from the associated power profile (see Figs. 5–7) the good dynamic behavior during different periods under various load changes. This confirms the effectiveness of the proposed strategy under the disturbance of load change condition.

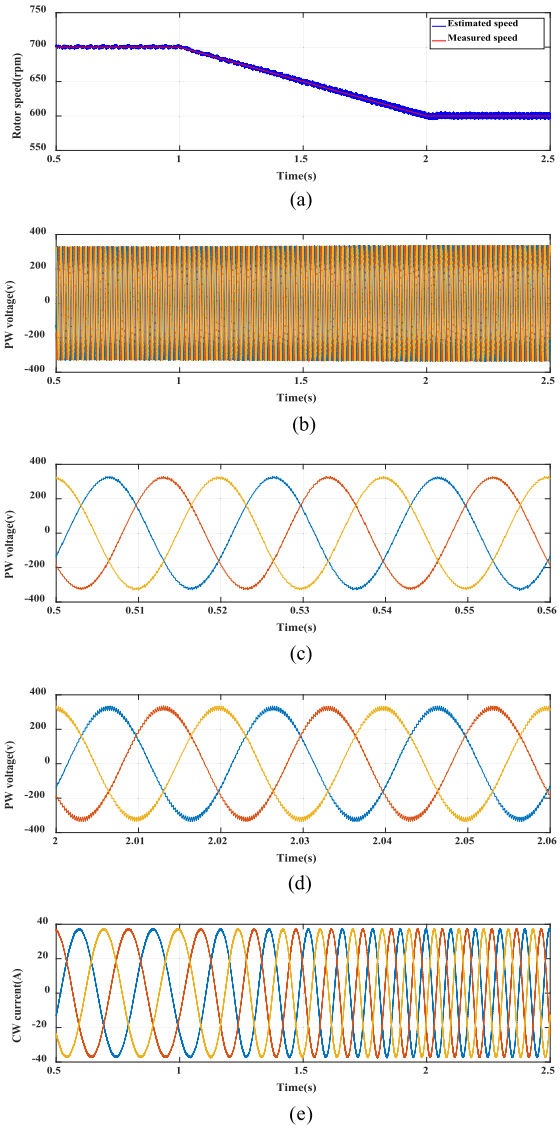

Fig. 4. Simulation results under the speed ramp change with the constant load. (a) Actual and estimated rotor speeds. (b) PW three-phase voltages. (c) Detailed PW three-phase voltages between 0.5 and 0.56 s. (d) Detailed PW three-phase voltages between 2 and 2.06 s. (e) CW three-phase currents.

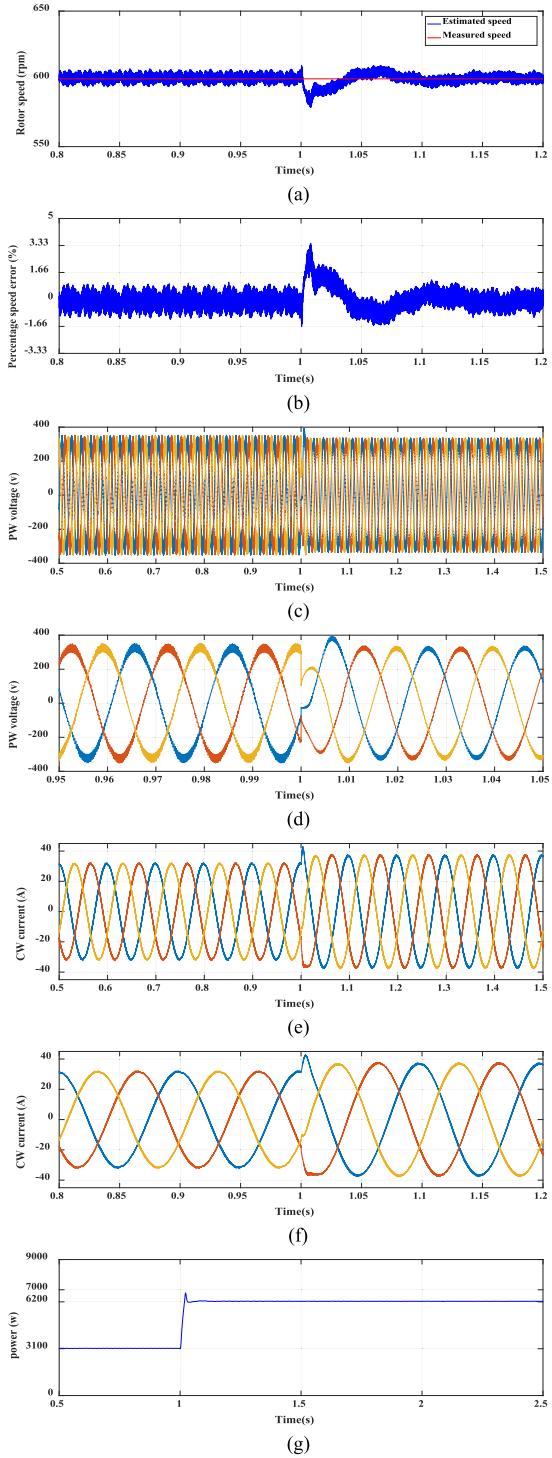

Fig. 5. Simulation results under load change at the constant rotor speed. (a) Actual and estimated rotor speeds. (b) Speed percentage error. (c) PW three-phase voltages. (d) Detailed view of PW three-phase voltages. (e) CW three-phase currents. (f) Detailed view of CW three-phase currents. (g) PW active power.

Moreover, it is noticed from the simulation results, as shown in Figs. 6 and 7, that the proposed sensorless control strategy is not affected by any variation in the BDFIG parameters including both the PW resistance and the inductances, but they affect the estimation of the generator speed.

The study presented in this section well illustrates the capability of the proposed sensorless control strategy based on the CW-flux MRAS observer for the DVC of the stand-alone BDFIG systems with good transient responses.

VI. Experimental Results

Comprehensive experiments are carried out to verify the effectiveness of the proposed sensorless control method based on the CW-flux MRAS observer. Fig. 8 illustrates the experimental setup of the stand-alone wound-rotor BDFIG system. This prototype consists of a wound-rotor BDFIG, a prime mover of 37-kW induction motor, a back-to-back converter integrated with DSP TMS28335 control circuit for interconnecting the PW and CW, and load box. The parameters of the BDFIG system are listed in Table I.

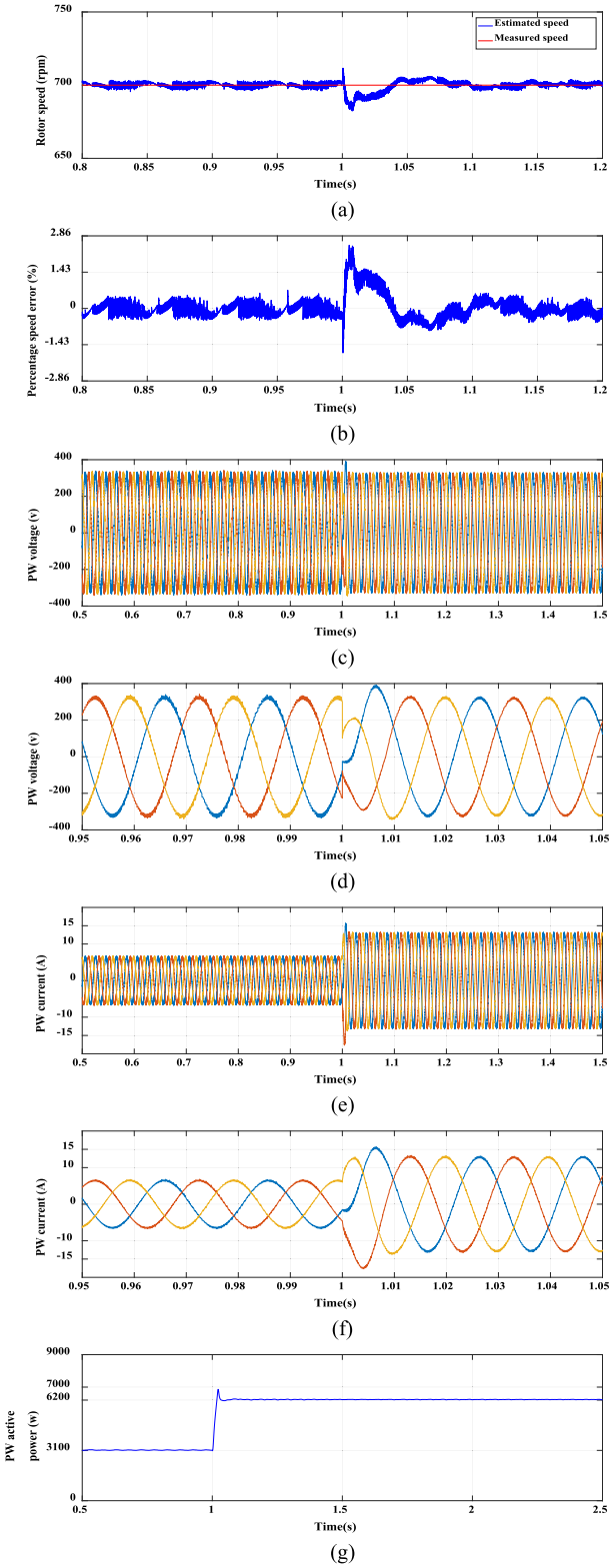

Fig. 6. Simulation results under 130% variation in the PW resistance. (a) Actual and estimated rotor speeds. (b) Speed percentage error. (c) PW three-phase voltages. (d) Detailed view of PW three-phase voltages. (e) PW three-phase currents. (f) Detailed view of PW three-phase currents. (g) PW active power.

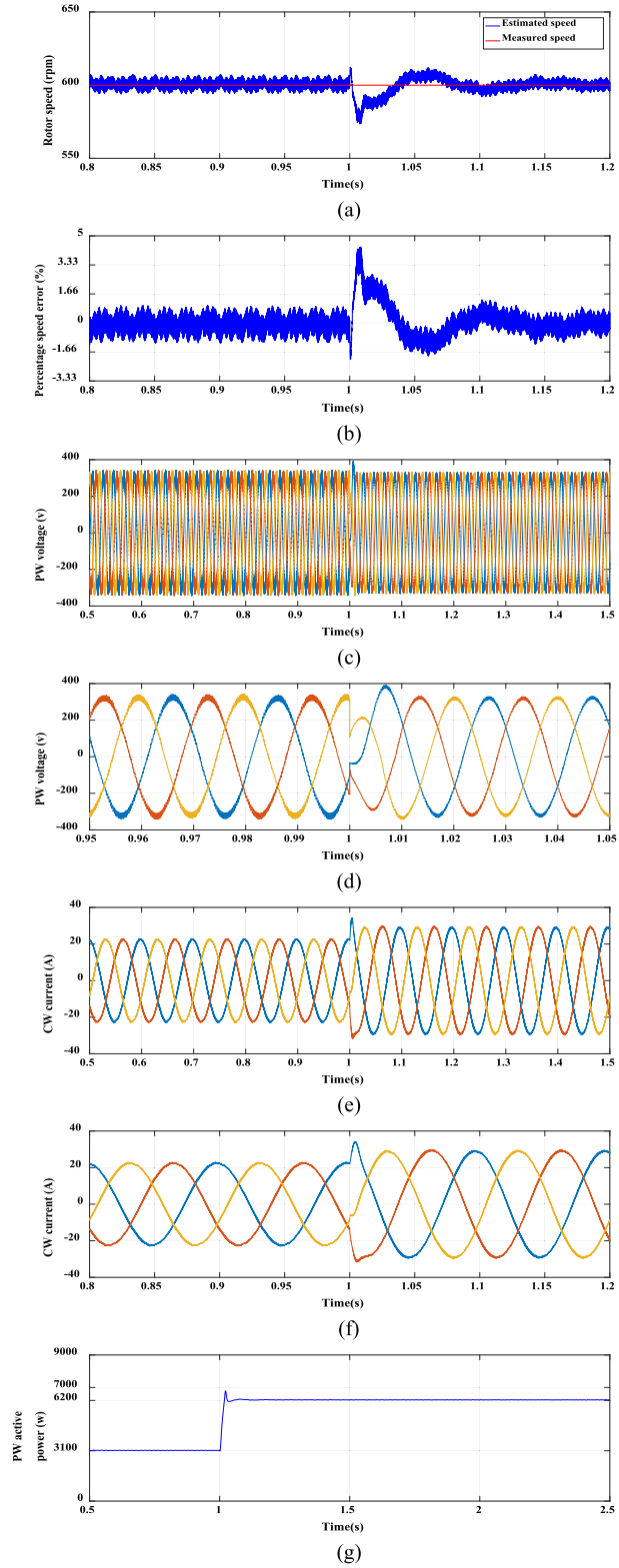

Fig. 7. Simulation results under 150% variation in the whole inductance. (a) Actual and estimated rotor speeds. (b) Speed percentage error. (c) PW three-phase voltages. (d) Detailed view of PW three-phase currents. (e) CW three-phase currents. (f) Detailed view of CW three phase. (g) PW active power.

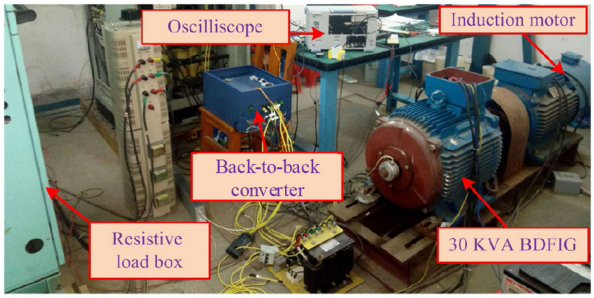

Fig. 8. Photograph of the experimental setup.

A. Variable Speed and Constant Load

The generator speed started from 700 r/min under a three-phase load of 50 Ω per phase and then is reduced to 600 r/min. Fig. 9(a) illustrates the estimated speed by the proposed speed observer, which well tracks the actual speed. Fig. 9(b) shows the error between the actual and the estimated speed. The control strategy succeeded in keeping the load voltage constant at the reference rms value of 150 V, as confirmed in Fig. 9(c). The CW current under different speeds is shown in Fig. 9(d), and the estimated speed can be verified by the frequency of winding current, as illustrated in Fig. 9(e) and (f).

B. Variable Load Under Constant Speed

When the generator speed is fixed at 600 r/min and the load is initially set at 50 Ω per phase and then decreased to 25 Ω per phase, both the actual and estimated speed are shown in Fig. 10(a), and the difference between them (error) is illustrated in Fig. 10(b). As shown in Fig. 10(c), the output voltage of the PW is fixed at 150 V rms. Fig. 10(d) shows the zoomed waveform of the PW voltage to show that the frequency is maintained at 50 Hz. The CW current and the zoomed waveform are shown in Fig. 10(e) and (f), respectively.

C. Variable Speed and Variable Load With 1.5L Variation

The third experimental test is carried out with the variable speed, variable load, and 1.5 increases in all inductances. The generator is initially operated at 700 r/min with a three-phase load of 50 Ω per phase. Then, the speed is reduced to 600 r/min and during the decrease of the speed, the terminal load is changed from 50 to 25 Ω per phase. As shown in Fig. 11(a), the estimated speed well tracks the actual speed during the load and speed variation. The error is about 0.6% from the reference speed, as shown in Fig. 11(b). The PW terminal load voltage and the CW current are illustrated in Fig. 11(c) and (d). The effect of load change can be observed from the CW current, as shown in Fig. 11(d).

D. Response With Load Variation Under PW Resistance Variation ($1.3R_1$)

To illustrate the effects of parameter variations, e.g., the PW resistance, the fourth experimental test is carried out at a constant speed with variable load. The generator is initially operated at

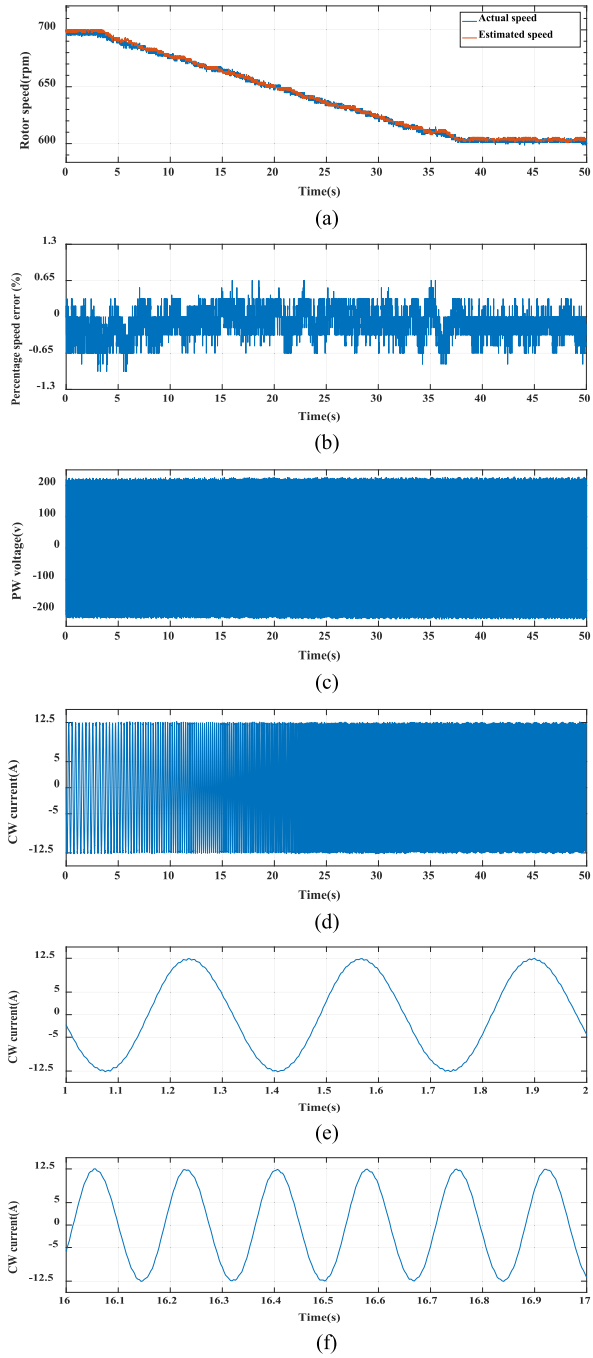

Fig. 9. Experimental results under variable speed (700 r/min to 600 r/min speed change). (a) Actual and estimated rotor speed. (b) Speed percentage error. (c) PW phase voltage. (d) Overall CW phase current. (d) Detailed CW phase current between 1 and 2 s. (d) Detailed CW phase current between 16 and 17 s.

700 r/min with the three-phase load of 50 Ω per phase. At 1.8 s, the terminal load is changed from 50 to 25 Ω per phase, as shown in Fig. 12. Although the PW circuit resistance changes, the proposed estimation method is capable of correctly estimating the actual speed, as confirmed by Fig. 12(a). The error between the estimated and measured speeds is plotted in Fig. 12(b). The maximum value of this error is less than 0.6% from the reference speed. The detailed PW load voltage is illustrated in Fig. 12(c) and (d) (zoomed waveform). The effect of load change can be

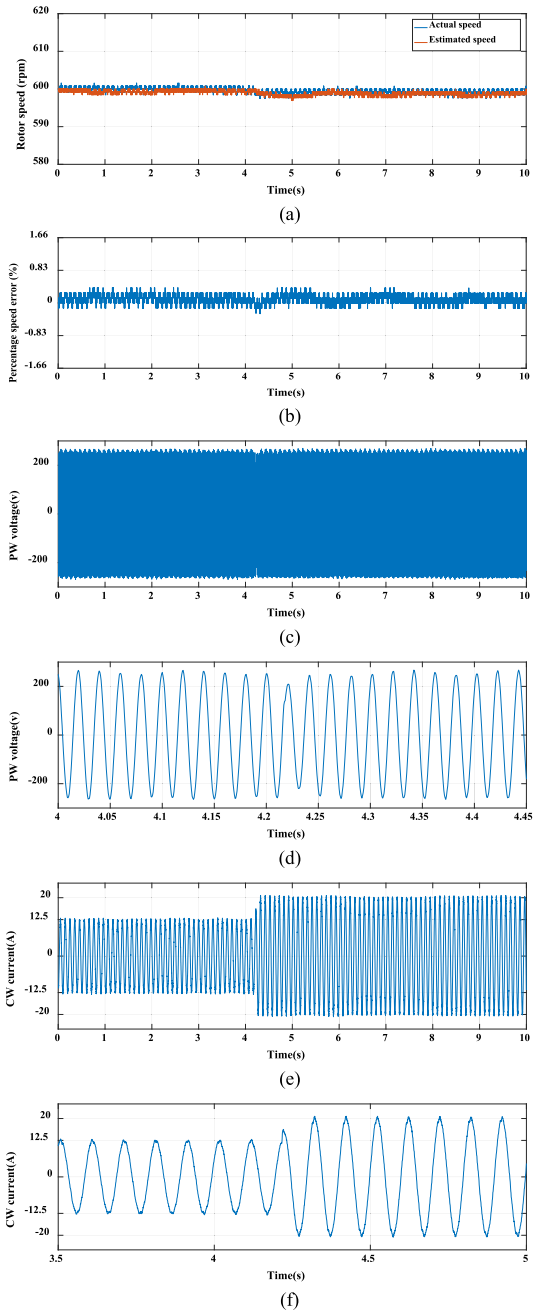

Fig. 10. Experimental results under variable load at the rotor speed of 600 r/min. (a) Actual and estimated rotor speeds. (b) Speed percentage error. (c) Overall PW phase voltage. (d) Detailed PW phase voltage between 4 and 4.45 s. (e) Overall CW phase current. (f) Detailed PW phase current between 3.5 and 5 s.

observed from the PW current, as shown in Fig. 12(e) and (f) (zoomed waveform).

E. Load Variation and Constant Speed Under 1.5 Increase of All Inductances of BDFIG

In this section, the effectiveness of the proposed MRAS is tested under strong variations when all inductances are increased by 1.5 times of the rated values. These increases in inductances are set from the starting process. The experimental test is studied

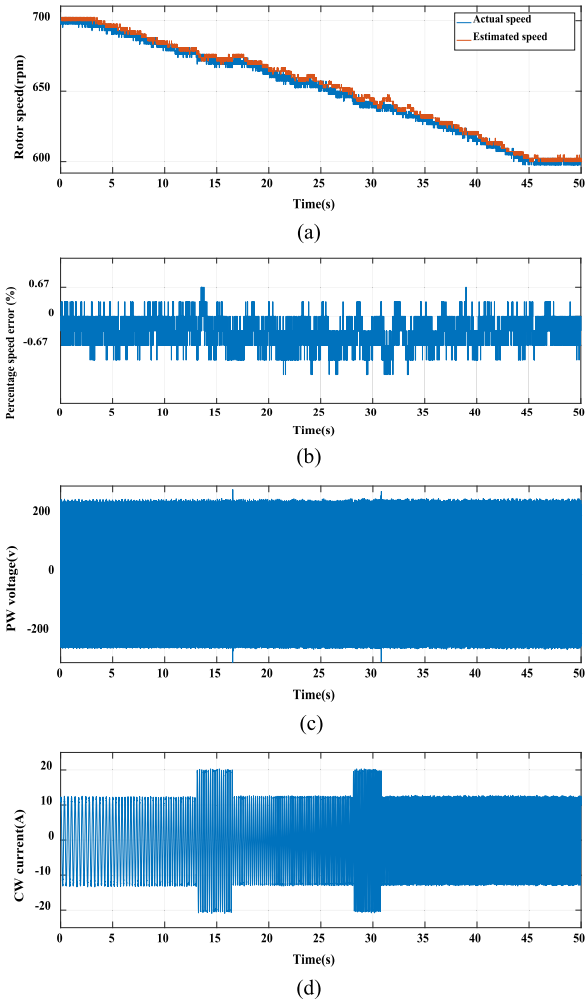

Fig. 11. Experimental results under variable speed (700 r/min to 600 r/min speed change and load change at the same time) with inductance variation. (a) Actual and estimated rotor speed. (b) Speed percentage error. (c) PW phase voltage. (d) CW phase current.

at a constant speed of 700 r/min and the load changes from 50 to 25 Ω per phase. Fig. 13(a) illustrates the estimated and actual speeds during load variation. Fig. 13(b) plots the error of speed tracking. Fig. 13(c) and (d) (zoomed waveform) shows the phase-A instantaneous PW voltage, whose peak value is 212 V corresponding to 150 V rms. The output frequency can be observed from the detailed PW voltage, as shown in Fig. 13(d). The CW current and the zoomed plot are presented in Fig. 13(e) and (f), respectively, to illustrate the effect of load change.

F. Speed Change and Constant Load Under Inductance Variation for All Generator Inductances

To validate the proposed control strategy, the sixth experimental test is presented, as shown in Fig. 14, with variable speed from 700 to 600 r/min, fixed load at 50 Ω per phase, and 150% increase in all inductances.

All the experimental results of this case study are plotted in Fig. 14(a)–(f), illustrating the actual and estimated speeds, the error of speed tracking, the real time and zoomed waveforms

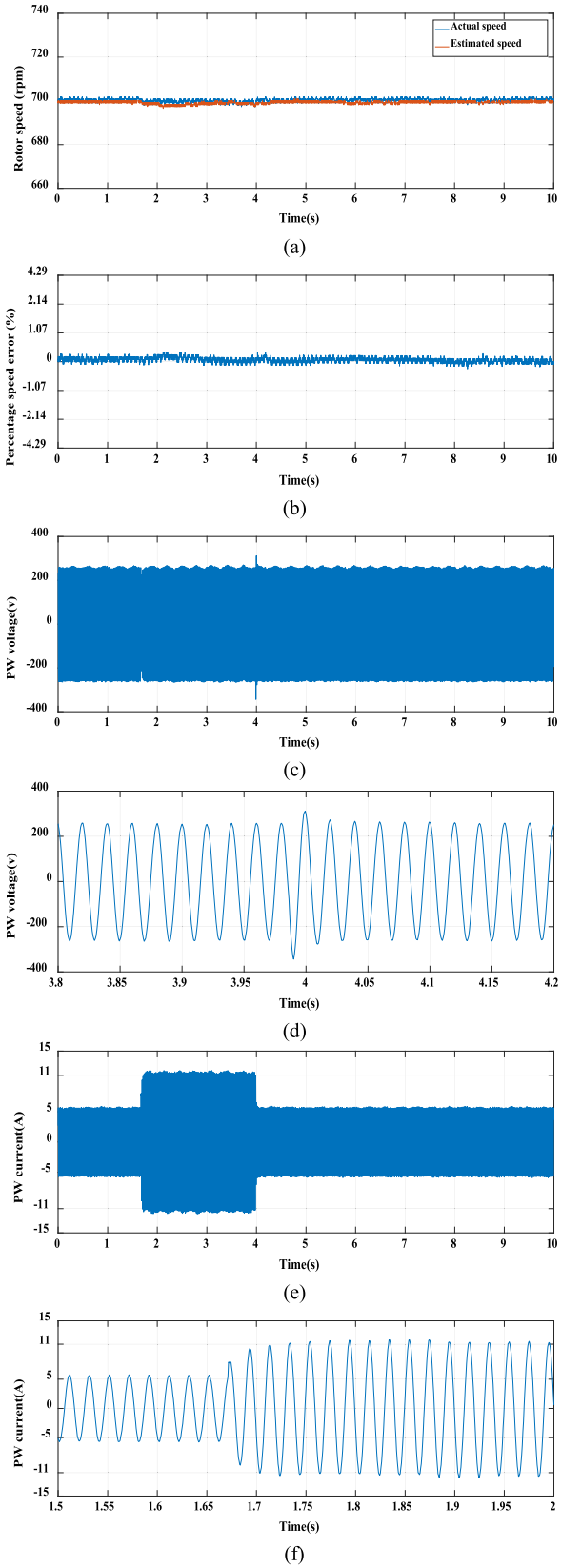

Fig. 12. Experimental results under PW resistance variation at the speed of 700 r/min. (a) Actual and estimated rotor speeds. (b) Speed percentage error. (c) Overall PW phase voltage. (d) Detailed PW phase voltage between 3.8 and 4.2 s. (e) Overall PW phase current. (f) Detailed PW phase current between 1.5 and 2 s.

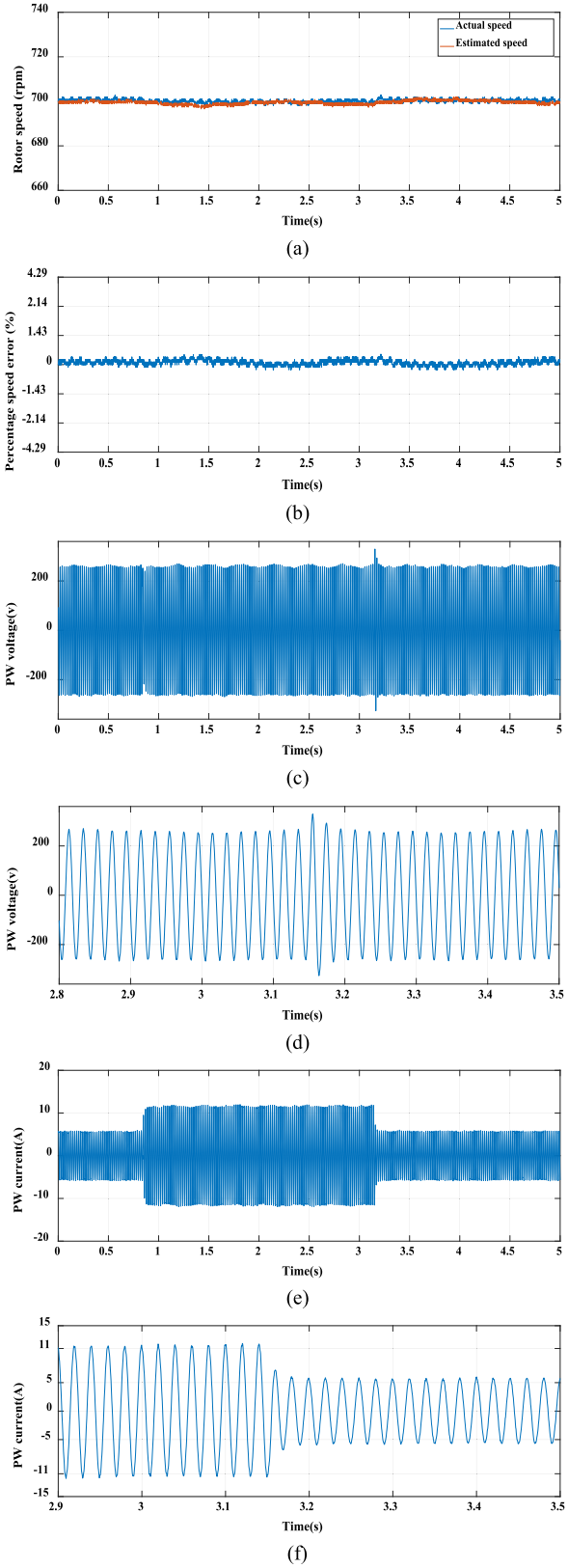

Fig. 13. Experimental results under inductance variation at the speed of 700 r/min. (a) Actual and estimated rotor speeds. (b) Speed percentage error. (c) Overall PW phase voltage. (d) Detailed PW phase voltage between 2.8 and 3.5 s. (e) Overall PW phase current. (f) Detailed PW phase current between 2.9 and 3.5 s.

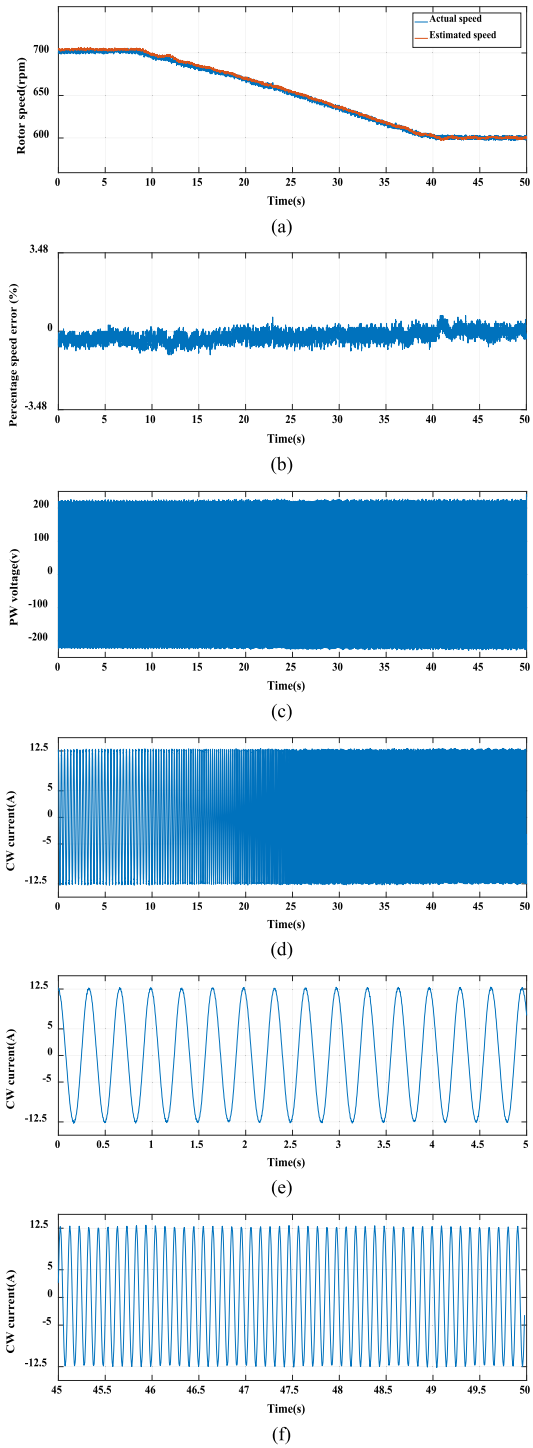

Fig. 14. Experimental results under speed change and constant load with inductance variation. (a) Actual and estimated rotor speed. (b) Speed percentage error. (c) PW phase voltage. (d) Overall CW phase current. (e) Detailed CW phase current between 0 and 5 s. (f) Detailed CW phase current between 45 and 50 s.

of the PW voltage and CW current, respectively. As shown by the presented experimental results, the proposed sensorless control method is not affected by any mismatch in the BDFIG parameters, including both the PW resistances and inductances. Both the simulation and experimental results confirm that the estimated generator speed can successfully track the actual value under different operating conditions, and the proposed sensorless control method based on the CW-flux MRAS is effective for the stand-alone BDFIG systems.

VII. Conclusion

This article presents a new MRAS speed observer based on the CW flux for the sensorless control of stand-alone BDFIGs. The effectiveness of the presented control method is illustrated by simulation results and verified by experiments. The tested BDFIG has demonstrated good transient behavior under different rotor speeds, load variations, and parameter changes under the control of the proposed control method based on the CW-flux MRAS. The results also demonstrate good tracking between the estimated and actual speed response, demonstrating the strong capability of the proposed sensorless control based on the CW-flux MRAS observer for the stand-alone BDFIGs.

References

[1] A. Oraee, E. Abdi, and R. A. McMahon, "Converter rating optimisation for a brushless doubly fed induction generator," *IET Renewable Power Gener.*, vol. 9, no. 4, pp. 360–367, May 2015.

[2] J. Chen, W. Zhang, B. Chen, and Y. Ma, "Improved vector control of brushless doubly fed induction generator under unbalanced grid conditions for offshore wind power generation," *IEEE Trans. Energy Convers.*, vol. 31, no. 1, pp. 293–302, Mar. 2016.

[3] H. Gorginpour, H. Oraee, and R. A. McMahon, "A novel modeling approach for design studies of brushless doubly fed induction generator based on magnetic equivalent circuit," *IEEE Trans. Energy Convers.*, vol. 28, no. 4, pp. 902–912, Dec. 2013.

[4] X. Wang, H. Lin, and Z. Wang, "Transient control of the reactive current for the line-side converter of the brushless doubly-fed induction generator in stand-alone operation," *IEEE Trans. Power Electron.*, vol. 32, no. 10, pp. 8193–8203, Oct. 2017.

[5] G. Tarchała and T. Orłowska-Kowalska, "Equivalent-signal-based sliding mode speed MRAS-type estimator for induction motor drive stable in the regenerating mode," *IEEE Trans. Ind. Electron.*, vol. 65, no. 9, pp. 6936–6947, Sep. 2018.

[6] M. Szypulski and G. Iwanski, "Sensorless state control of stand-alone doubly fed induction generator supplying nonlinear and unbalanced loads," *IEEE Trans. Energy Convers.*, vol. 31, no. 4, pp. 1530–1538, Dec. 2016.

[7] A. Pal, S. Das, and A. K. Chattopadhyay, "An improved rotor flux space vector based MRAS for field-oriented control of induction motor drives," *IEEE Trans. Power Electron.*, vol. 33, no. 6, pp. 5131–5141, Jun. 2018.

[8] Y. Liu, W. Ai, B. Chen, K. Chen, and G. Luo, "Control design and experimental verification of the brushless doubly-fed machine for stand-alone power generation applications," *IET Elect. Power Appl.*, vol. 10, no. 1, pp. 25–35, Jan. 2016.

[9] Y. Liu, W. Ai, B. Chen, and K. Chen, "Control design of the brushless doubly-fed machine for stand-alone VSCF ship shaft generator systems," *J. Power Electron.*, vol. 16, no. 1, pp. 259–267, Jan. 2016.

[10] X. Wei, M. Cheng, W. Wang, P. Han, and R. Luo, "Direct voltage control of dual-stator brushless doubly fed induction generator for stand-alone wind energy conversion systems," *IEEE Trans. Magn.*, vol. 52, no. 7, Jul. 2016, Art. no. 8203804.

[11] M. G. Hussien, W. Xu, and Y. Liu, "Vector control schemes for direct voltage control of the stand-alone brushless doubly-fed induction generator," in *Proc. 21st Int. Conf. Elect. Mach. Syst.*, Jeju, South Korea, 2018, pp. 1307–1312.

[12] R. Cardenas, R. Pena, J. Clare, G. Asher, and J. Proboste, "MRAS observers for sensorless control of doubly-fed induction generators," *IEEE Trans. Power Electron.*, vol. 23, no. 3, pp. 1075–1084, May 2008.

[13] R. Pena, R. Cardenas, J. Proboste, G. Asher, and J. Clare, "Sensorless control of doubly-fed induction generators using a rotor-current-based MRAS observer," *IEEE Trans. Ind. Electron.*, vol. 55, no. 1, pp. 330–339, Jan. 2008.

[14] M. Pattnaik and D. Kastha, "Adaptive speed observer for a stand-alone doubly fed induction generator feeding nonlinear and unbalanced loads," *IEEE Trans. Energy Convers.*, vol. 27, no. 4, pp. 1018–1026, Dec. 2012.
[15] Y. Zhu, X. Zhang, C. Liu, and H. Chen, "Study on speed sensorless control of brushless doubly-fed wind power generator based on flux linkage of the power winding," in *Proc. 7th Int. Power Electron. Motion Control Conf.*, Harbin, China, 2012, pp. 2453–2456.
[16] Y. Liu, W. Xu, F. Xiong, and F. Blaabjerg, "Sensorless direct voltage control of the stand-alone brushless doubly-fed generator," in *Proc. 20th Int. Conf. Elect. Mach. Syst.*, Sydney, NSW, Australia, 2017, pp. 1–6.
[17] W. Xu, D. Dong, Y. Liu, K. Yu, and J. Gao, "Improved sensorless phase control of stand-alone brushless doubly-fed machine under unbalanced loads for ship shaft power generation," *IEEE Trans. Energy Convers.*, vol. 33, no. 4, pp. 2229–2239, Dec. 2018.
[18] Y. Liu, W. Xu, T. Long, and F. Blaabjerg, "An improved rotor speed observer for standalone brushless doubly-fed induction generator under unbalanced and nonlinear loads," *IEEE Trans. Power Electron.*, vol. 35, no. 1, pp. 775–788, Jan. 2020.
[19] Y. Liu, W. Xu, J. Zhu, and F. Blaabjerg, "Sensorless control of standalone brushless doubly fed induction generator feeding unbalanced loads in a ship shaft power generation system," *IEEE Trans. Ind. Electron.*, vol. 66, no. 1, pp. 739–749, Jan. 2019.
[20] A. K. Ebraheem, W. Xu, Y. Liu, and M. G. Hussien, "Sensorless direct voltage control based on MRAS observer for the stand-alone brushless doubly-fed induction generator," in *Proc. 21st Int. Conf. Elect. Mach. Syst.*, Jeju, South Korea, 2018, pp. 1606–1611.
[21] J. Yang *et al.*, "Sensorless control of brushless doubly fed induction machine using a control winding current MRAS observer," *IEEE Trans. Ind. Electron.*, vol. 66, no. 1, pp. 728–738, Jan. 2019.

Wei Xu (M'09–SM'13) received the double B.E. and M.E. degrees from Tianjin University, Tianjin, China, in 2002 and 2005, respectively, and the Ph.D. degree from the Institute of Electrical Engineering, Chinese Academy of Sciences, Beijing, China, in 2008, all in electrical engineering.

From 2008 to 2012, he held several academic positions in both Australian and Japanese universities and companies. Since 2013, he has been a Full Professor with the State Key Laboratory of Advanced Electromagnetic Engineering and Technology, Huazhong University of Science and Technology, Wuhan, China. His research topics mainly cover design and control of linear/rotary machines.

Dr. Xu is a fellow of the Institute of Engineering and Technology. He has served as an Associate Editor for several journals, such as IEEE TRANSACTIONS ON INDUSTRIAL ELECTRONICS, IEEE JOURNAL OF EMERGING AND SELECTED TOPICS IN POWER ELECTRONICS, and IEEE TRANSACTIONS ON VEHICULAR TECHNOLOGY.

Alameen K. Ebraheem received the B.Sc. degree in electrical and electronic engineering from Nile Valley University, Atbara, Sudan, in 2008, and the M.Sc. degree in electrical engineering from the Sudan University of Science and Technology, Khartoum, Sudan, in 2012. Since September 2016, he has been working toward the Ph.D. degree with the State Key Laboratory of Advanced Electromagnetic Engineering and Technology, School of Electrical and Electronic Engineering, Huazhong University of Science and Technology, Wuhan, China.

He was appointed as a Lecturer at the Department of Electrical and Electronic Engineering, Faculty of Engineering and Technology, Nile Valley University, Atbara, Sudan, in 2012. His current research interests include sensorless control, control engineering, ac electrical machine control, and electrical drives.

Yi Liu (M'14) received the B.E. and M.E. degrees in automation and control engineering from the Wuhan University of Science and Technology, Wuhan, China, in 2004 and 2007, respectively, and the Ph.D. degree in mechatronic engineering from the Huazhong University of Science and Technology, Wuhan, China, in 2016.

From 2007 to 2011, he was a Lecturer with the City College, Wuhan University of Science and Technology, Wuhan, China. From March 2016 to June 2016, he was a Senior R&D Engineer with the Fourth Academy of China Aerospace Science and Industry Group, Wuhan, China. In July 2016, he became a Postdoctoral Research Fellow with the State Key Laboratory of Advanced Electromagnetic Engineering and Technology, School of Electrical and Electronic Engineering, Huazhong University of Science and Technology.

His current research interests include ac electrical machine control and inverter systems.

Jianguo Zhu (S'93–M'96–SM'03) received the B.E. degree from the Jiangsu Institute of Technology, Jiangsu, China, in 1982, the M.E. degree from the Shanghai University of Technology, Shanghai, China, in 1987, and the Ph.D. degree from the University of Technology Sydney (UTS), Sydney, Australia, in 1995, all in electrical engineering.

He was a Lecturer with UTS in 1994, promoted to a Full Professor in 2004, and a Distinguished Professor of electrical engineering in 2017. In 2018, he joined the University of Sydney, Australia, as a Full Professor and Head with the School of Electrical and Information Engineering. His research interests include computational electromagnetics, measurement and modeling of magnetic properties of materials, electrical machines and drives, power electronics, renewable energy systems, and smart microgrids.

Mohamed G. Hussien was born in Zefta, Gharbeya, Egypt, in 1988. He received the B.Sc. and M.Sc. degrees in electrical engineering from Tanta University, Tanta, Egypt, in 2011 and 2016, respectively. He is currently working toward the Ph.D. degree with the State Key Laboratory of Advanced Electromagnetic Engineering and Technology, School of Electrical and Electronic Engineering, Huazhong University of Science and Technology, Wuhan, China.

Since 2016, he has been an Assistant Lecturer with the Department of Electrical Power and Machines Engineering, Faculty of Engineering, Tanta University, Tanta, Egypt. His research interests include electrical machines analysis, electrical drives, sensorless control, power electronics, and renewable energy.

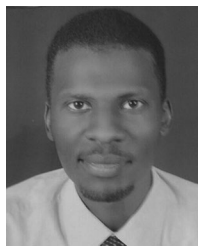

Omer Mohammed Elbabo Mohammed received the B.Sc. degree from the University of Kordofan, EL-Obied, Sudan, in 2010, and the M.Sc. degree from the Sudan University of Science and Technology, Khartoum, Sudan, in 2013, all in electrical engineering. Since September 2016, he has been working toward the Ph.D. degree with the State Key Laboratory of Advanced Electromagnetic Engineering and Technology, School of Electrical and Electronic Engineering, Huazhong University of Science and Technology, Wuhan, China.

He was a Lecturer with the Department of Electrical Engineering, Faculty of Engineering, University of Sinnar, Sinnar, Sudan, in 2013. His current research interests include ac electrical machine control and power quality issues.